Transition Experiments on Large Bluntness Cones with Distributed Roughness in Hypersonic Flight

Daniel C. Reda* and Michael C. Wilder†
NASA-Ames Research Center, Moffett Field, CA 94035-1000

and

Dinesh K. Prabhu‡
ERC, Inc., Moffett Field, CA 94035-1000

Large bluntness cones with smooth nosetips and roughened frusta were flown in the NASA Ames hypersonic ballistic range at a Mach number of 10 through quiescent air environments. Global surface intensity (temperature) distributions were optically measured and analyzed to determine transition onset and progression over the roughened surface. Real-gas Navier-Stokes calculations of model flowfields, including laminar boundary layer development in these flowfields, were conducted to predict values of key dimensionless parameters used to correlate transition on such configurations in hypersonic flow. For these large bluntness cases, predicted axial distributions of the roughness Reynolds number showed (for each specified freestream pressure) that this parameter was a maximum at the physical beginning of the roughened zone and decreased with increasing run length along the roughened surface. Roughness-induced transition occurred downstream of this maximum roughness Reynolds number location, and progressed upstream towards the beginning of the roughened zone as freestream pressure was systematically increased. Roughness elements encountered at the upstream edge of the roughened frusta thus acted like a finite-extent "trip array", consistent with published results concerning the tripping effectiveness of roughness "bands" placed on otherwise smooth surfaces.

Nomenclature

D_B = model base diameter
k = 3D roughness element height
$\bar{k}$ = average roughness element height for distributed roughness
L = model length
M = Mach number
P = static pressure in ballistic range
R_N = model nose tip radius
Re_{kk} = roughness Reynolds number, $\frac{\rho_k u_k \bar{k}}{\mu_w}$
T = temperature
u = fluid velocity
V = model velocity
X = model axial length measured from tip along centerline
δ = boundary layer thickness
θ = boundary layer momentum thickness
θ_c = cone frustum half angle

* Senior Research Scientist, Aerothermodynamics Branch, MS 230-2; Fellow, AIAA.
† Senior Research Scientist, Aerothermodynamics Branch, MS 230-2; Associate Fellow, AIAA.
‡ Senior Research Scientist, ERC, Inc.; Associate Fellow, AIAA.

μ = fluid viscosity
ρ = fluid density
ϕ = flow-aligned polar coordinate on hemisphere surface measured from stagnation point

Subscripts
e = based on conditions at laminar boundary layer edge
k = based on conditions in the laminar boundary layer at the roughness height
max = value at start of roughness
0 = at the stagnation point
TR = at transition location
w = based on wall conditions
∞ = freestream

I. Introduction

BOUNDARY layer transition, aside from being one of the classical unsolved problems of basic fluid physics, remains a real-world problem for designers of advanced flight systems. Accurate predictions of viscous flowfields around high-speed aircraft, missiles, and entry vehicles are of paramount importance to each system's design and subsequent flight performance. Boundary layer transition is known to affect vehicle dynamics, drag, and surface heat transfer rates significantly.

In the hypersonic flow regime, thermal protection of flight vehicles is often accomplished with ablating heat shields. In such cases, frictional energy generated between the flight vehicle and its atmospheric environment is absorbed, and shed as the thermal protection system (TPS) ablates and recedes.

Ablating TPS on planetary entry trajectories first experience thermochemistry under high-altitude, low-Reynolds-number conditions. Such laminar flow ablation causes the formation of a distributed surface microroughness pattern characteristic of the TPS material composition and fabrication process. Once formed, these distributed surface roughness elements create disturbances within the laminar boundary layer flowing over the surface. As altitude decreases, Reynolds number increases, and flowfield conditions capable of amplifying these roughness-induced perturbations are eventually achieved, that is, transition onset occurs. Boundary layer transition to turbulence results in more severe heat transfer rates and accelerated surface recession.

Overly conservative TPS designs may result from assuming fully turbulent flow throughout the entire entry trajectory; in such cases, transition onset and progression over the TPS surface are ignored. The drawback of this limiting approach is that the "required" heat shield mass can become excessive; the overall weight penalty could thus force other components of the vehicle to be minimized or eliminated entirely. A more rigorous approach is made possible if a validated physical model for roughness-induced transition onset and progression is developed for the TPS material/geometry of interest. Safety factors must still be applied in the thermal analysis, but overall TPS mass is thus more realistically defined.

Early manned entry vehicles were blunt capsules with ablating TPS in the shape of a sphere segment. Unmanned planetary entry vehicles are generally axisymmetric in shape: slightly-blunted slender cones for strategic weapons applications and large-bluntness large-angle cones for planetary exploration applications. Complicating the designs of such vehicles, the nose tips or nose caps can be comprised of ablative materials different from those deployed on the downstream conic sections.

Early transition research on smooth and rough bodies at hypersonic speeds was conducted in conventional hypersonic wind tunnels. However, it soon became apparent that transition physics was adversely affected by facility noise, both convected along the freestream from plenum chambers, and radiated into the freestream from turbulent boundary layers on the nozzle walls. The evolution of this understanding is covered in Refs. 1 through 7. A coordinated national effort to overcome these testing limitations was put forward by Reshotko,[8] involving the development and use of quiet supersonic and hypersonic wind tunnels, supplemented by experiments in quiet ballistic ranges and in atmospheric flight tests. A recent review on this subject is given by Schneider.[9] Results of ballistic range transition experiments using smooth-wall conical models launched at supersonic and hypersonic speeds were reported by Sheetz,[10-12] Potter,[13, 14] and Reda.[15] Effects of distributed roughness on blunt body transition at hypersonic speeds were investigated in the ballistic range experiments of Reda.[16-19] Most recently, effects of isolated roughness elements on blunt body transition in hypersonic free flight were reported.[20]

A review of roughness-dominated transition correlations for reentry applications was given by Reda.[21] Based on analyses of published correlations for blunt bodies, attachment lines, and windward surfaces of lifting entry vehicles, it was found that all of these transition correlations could be recast into and be well modeled by the critical

roughness Reynolds number concept. This concept is attributed to Schiller,[22] who hypothesized that, at some critical value, vortices would be shed from the top of the roughness element(s), causing an abrupt breakdown to turbulence. The critical Reynolds number was based on smooth-wall laminar boundary layer conditions at the roughness height, and the length scale was the roughness height. This modeling approach was further corroborated by analyses of roughness-dominated transition data bases obtained since this 2002 review.[19, 20]

It is acknowledged that the assumed breakdown mechanism stated above is simplistic and poorly understood. Both Reshotko and Tumin[23] and Schneider[24] have presented detailed discussions of potential breakdown mechanisms associated with surface roughness. However, a validated computational capability to predict roughness-dominated transition from first principles does not yet exist. Until such a predictive capability becomes available, the critical roughness Reynolds number correlating approach offers a semi-empirical methodology to designers of hypersonic flight vehicles.

Three transition modeling applications were addressed in recent and ongoing research at NASA-Ames: hemispheres with distributed roughness;[19] small-bluntness cones with smooth nosetips and roughened frusta;[25] and large-bluntness cones with smooth nosetips and roughened frusta (the present paper).

Summarizing current understanding, transition onset and progression over blunt (hemispherical) shapes with distributed surface roughness patterns induced by laminar ablation processes are well modeled by the critical roughness Reynolds number approach.[19] Figure 1 illustrates the sequence of events that occurs on a typical hypersonic planetary entry trajectory. Real-gas Navier-Stokes computations[26-28] were used to predict the distribution of the roughness Reynolds number (Re_{kk}) around the hemispherical shape at each of several freestream pressures. The critical value of 250 determined in Ref. 19 is first achieved at the sonic point, and, as the freestream pressure increases (altitude decreases) the intersection of the predicted Re_{kk} distribution with the critical value systematically moves forward through the subsonic edge Mach number region, towards the stagnation point. Figure 2 shows the transition correlation that resulted from this research.[19]

An identical trend was observed for transition onset and progression over roughened frusta of smooth-nosetip, small-bluntness cones in hypersonic free flight, cases wherein the edge Mach number above the roughened surface was supersonic.[25] Figure 3 shows results of real-gas Navier-Stokes computations used to predict roughness Reynolds number distributions over such a geometry. Employing a smooth nosetip ensured a known (computed) laminar boundary layer profile entering the roughened region. The critical value of Re_{kk} was unknown a priori, so a value of 250 was chosen as a pre-test estimate. As can be seen, for a small-bluntness tip, Re_{kk} values increase with increasing distance along the roughened frustum, reaching a maximum value at the base of the cone. If a critical value for Re_{kk} existed, transition onset would first be achieved at the cone base. Systematic increases in freestream pressure (reductions in effective altitude)

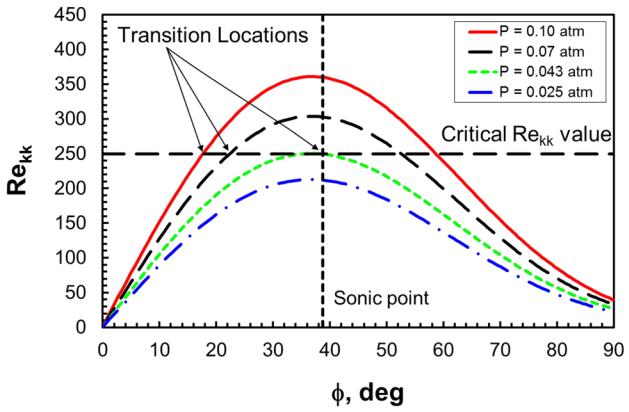

Figure 1. Transition onset on hemispherical shapes with distributed roughness occurs at the sonic point and progresses forward, towards the stagnation point, as freestream pressure (Reynolds number) increases. M_∞ = 12; R_N = 14.3 mm; $\bar{k}$ = 15.2 μm; gas = air; T_w = 900 K.

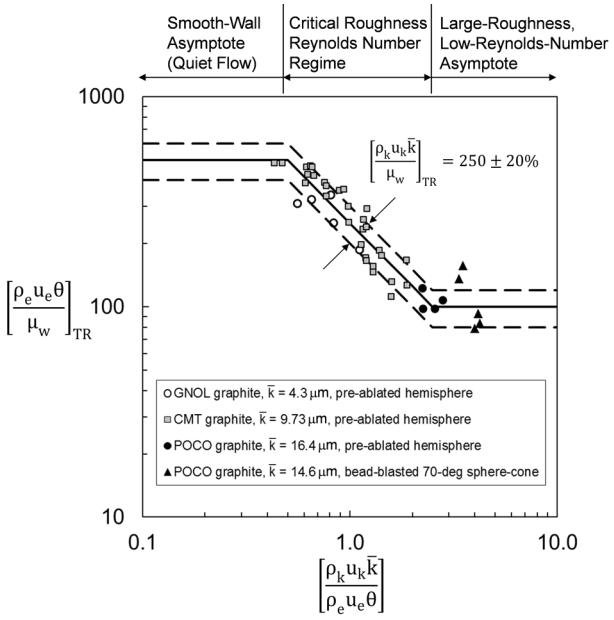

Figure 2. Transition correlation for blunt bodies with distributed roughness in hypersonic free flight.

would then cause the predicted crossing of the computed Re_{kk} distribution with the critical Re_{kk} value (the transition front location) to progress forward, towards the upstream-most location of the distributed roughness pattern. This trend was substantiated by experiment and results are shown in Fig. 4.[25] The critical value of the roughness Reynolds number for transition was found to be 266 ± 20%, in agreement with the critical value of 250 ± 20% for transition on rough blunt bodies.

What is unknown at this point is whether or not the critical roughness Reynolds number correlating approach can be extended with validity to roughened frusta of large-bluntness cones in hypersonic flow, cases wherein the laminar boundary layer development over the nosetip and onto the conic frustum is dominated by entropy swallowing effects. The present paper addresses this issue.

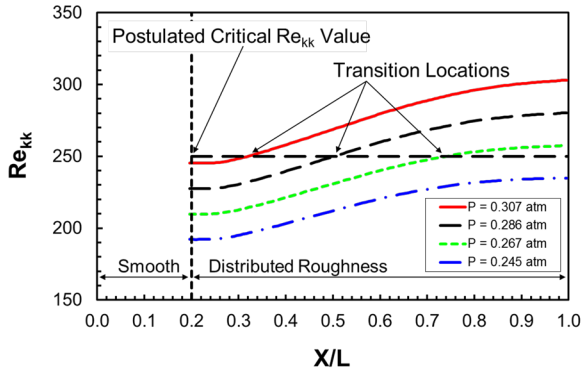

Figure 3. Transition onset on frusta of small-bluntness cones with distributed roughness occurs at the base and progresses forward, towards the beginning of the roughened region, as freestream pressure (Reynolds number) increases. $M_\infty = 10$; $R_N = 1.143$ mm; half angle = 30°; $\bar{k}$ = 5.6 μm; gas = air; Tw = 650 K.

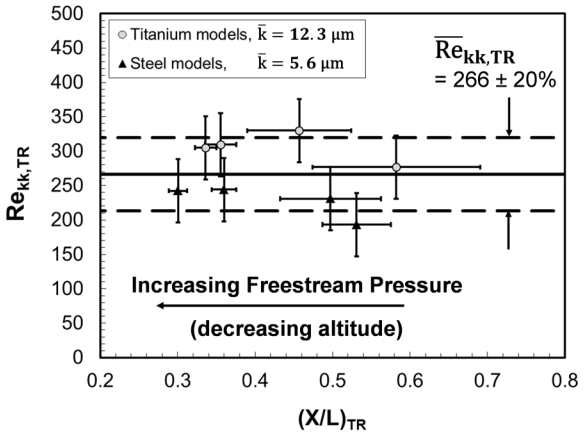

Figure 4. Transition front progression over roughened frusta of smooth-nosetip, small-bluntness cones, freestream pressure (freestream Reynolds number) increasing right to left.

II. Large-Bluntness Cones

The model geometry chosen for this phase of the research is summarized below:

θ_c = 30 degrees
R_N = 0.3 in (7.62 mm), smooth
D_B = 1.191 in (30.25 mm)
L = 0.739 in (18.77 mm)

Each model was machined from a single piece of stainless steel alloy (304). Figure 5(a) shows a photograph of a typical model, mounted in the launch sabot with one half of the sabot removed to reveal the full length of the model. Figure 5(b) shows a shadowgraph of this model in flight at $M_\infty = 10$.

The surface roughness distribution (starting at X/L = 0.2) was applied by the two-step bead-blasting procedure described in Ref. 25. Surface microroughness patterns were characterized by reflected white light interferometry[29] and results are identical to those reported in Ref. 25 (see Fig. 6). The mean roughness height was $\bar{k}$ = 5.6 μm. For the present experiments, the mean roughness height relative to the momentum thickness and boundary layer thickness at X/L = 0.2 were $0.419 \leq \bar{k}/\theta \leq 0.702$ and $0.058 \leq \bar{k}/\delta \leq 0.093$, respectively.

Pretest calculations were conducted to compute axial distributions of the roughness Reynolds number along the roughened frusta, with free stream static pressure as the parameter. To guide in the selection of test

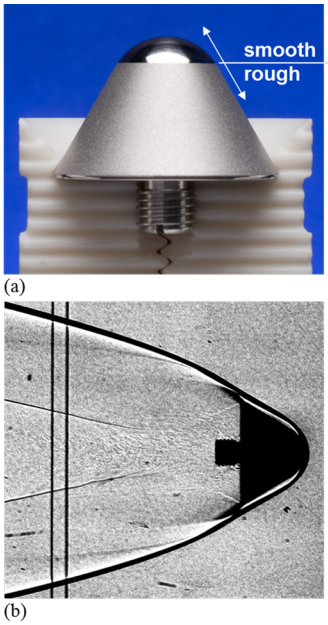

Figure 5. (a) Model mounted in launch sabot with two of four sabot fingers removed; (b) Model in flight at $M_\infty = 10$.

conditions, a critical Re_{kk} value of 250 was once again assumed. Results are shown in Fig. 7.

The primary difference between the slightly-blunted and large-bluntness cones is that the predicted distribution of Re_{kk} along the roughened surface decreases with increasing run length in the large-bluntness case. Thus, for a given freestream pressure, the predicted Re_{kk} distribution first exceeds the assumed critical value at the beginning of the roughness distribution (see the P = 0.267 atm curve of Fig. 7). If the Re_{kk} transition modeling approach is valid for such cases, transition onset would always occur at this location; there would be no forward progression of the transition front over the roughened surface with increasing freestream pressure as observed in the slightly-blunted cone experiments. In addition, the following question arose: if Re_{kk} at the start of the roughness exceeds some critical value, yet decreases below it in a short distance downstream, would tripping of the laminar boundary layer entering the roughened zone be "effective", or would input disturbances quickly die out (not be amplified)?

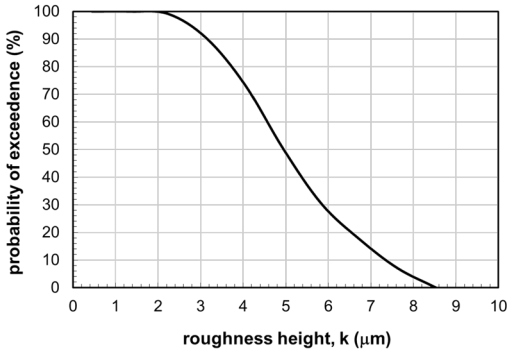

Figure 6. Measured surface roughness distribution, $\bar{k}$ = 5.6 μm.

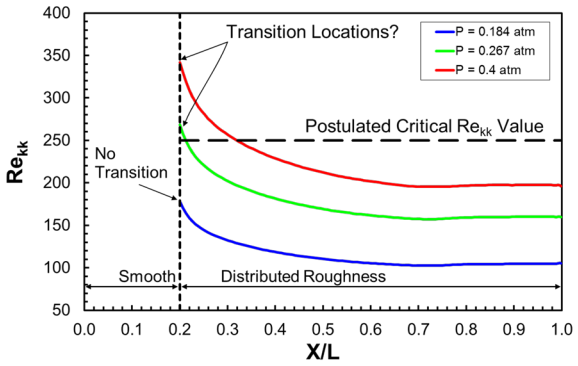

Figure 7. Roughness Reynolds number distributions on large-bluntness cones with distributed roughness. M_∞ = 10; R_N = 7.62 mm; half angle = 30°; $\bar{k}$ = 5.6 μm; gas = air; T_w = 550 K.

III. Experimental Approach

The experiments were performed in the Hypervelocity Free Flight Aerodynamic Facility at NASA Ames Research Center. The ballistic range, shown in Fig. 8, employs a two-stage light-gas gun to launch individual models on trajectories through a quiescent, controlled-atmosphere test section. The gun used has an inner diameter of 38.1 mm (1.5 in), and the test section is approximately 1 m across and 23 m long, measured from the first optical measurement station to the last. The models are in flight for an additional 10 m from the exit of the gun barrel to the first optical measurement station, during which time the launch sabot is separated from the model by aerodynamic forces and trapped in the separation tank. There are sixteen optical measurement stations, spaced 1.524 m (5 ft) apart, along the length of the test section. Each station is equipped with orthogonal-viewing parallel-light shadowgraph cameras and high-speed timers for recording the flight trajectories. Pitch and yaw angles were measured from orthogonal-view photographs taken at multiple stations along each range trajectory and were generally less than a few degrees.

Models described in Section II were launched without spin at a nominal velocity of 3.4 km/s (11,150 ft/s) into quiescent room temperature air, yielding a freestream Mach number of 10 and an edge Mach number between 1.6 and 1.73 over the roughened frusta, for the freestream pressures of these tests. Freestream static pressure was systematically varied over

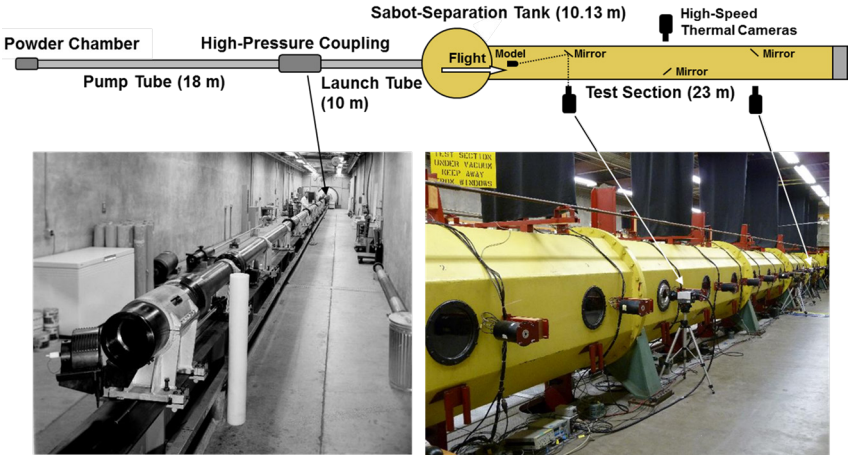

Figure 8. The NASA Ames Research Center free-flight ballistic range.

the range 0.143 atm ≤ P ≤ 0.4 atm in order to vary the primary independent variable Re_{kk}.

For these experiments, three of the optical measurement stations were equipped with high-speed thermal imaging infrared (IR) cameras to record the instantaneous global surface intensity distributions on the models: two cameras imaged one side of each model at the beginning and end of the range, respectively, while a third camera imaged the opposite side of each model at mid range. These infrared cameras were sensitive to the 3 – 5 μm infrared wavelength band. The cameras were located outside the test section, and viewed the models through anti-reflection-coated silicon windows, and off first-surface aluminum plane mirrors placed inside the test section, just off the line of flight, as illustrated in Fig. 8. An example image is shown in Fig. 9(a). The shock-layer gases of the bow shock radiate slightly in the IR wavelengths for the conditions of these experiments and have the potential to bias the surface temperature measurements. A localized plume of helium was created to temporarily quench this gas-cap radiation at each imaging station, as discussed in Ref. 30. The model was in the helium less than 0.5% of the total flight time, thus its effect on the integrated convective heating over the entire trajectory was minimal.

Camera calibration procedures outlined in Refs. 30 and 31 were employed to convert surface intensity images to global surface temperature images (see Fig. 9(b)). The response of each camera was calibrated against a blackbody radiation standard by imaging the blackbody source on an optical path equivalent to that employed in the ballistic-range tests. The standard deviation of temperature measurements of the calibration source was less than 5 K, for both spatial and temporal variations. All images were recorded with a 1 μs exposure time, and exposure level was controlled with neutral density filters having optical densities ranging for 0 to 1. The minimum detectable temperature was typically between 400 and 500 K, depending on the filter selection.

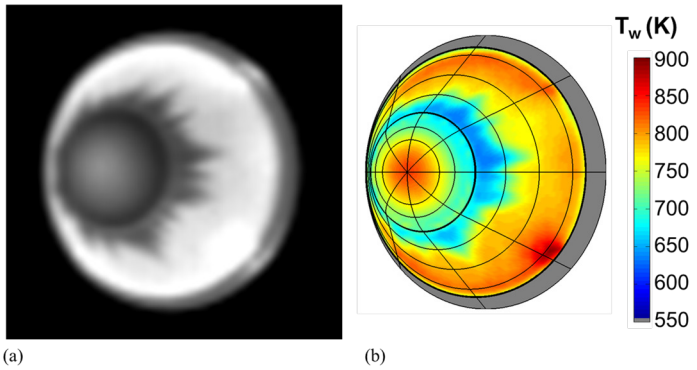

Figure 9. Oblique view of a stainless steel model, $M_\infty = 10$, P = 0.316 atm: (a) infrared image; (b) surface temperature distribution mapped to surface grid.

IV. Results

Results for the large-bluntness cone experiments are summarized in Fig. 10 and Fig. 11.

In Fig. 10 we show a sub-set of recorded thermal images to illustrate observed trends. For $Re_{kk,\,max} \leq 146$, no indications of any breakdown to turbulence on the roughened frusta were seen. At $Re_{kk,\,max} = 226$, turbulent wedges occurred near the aft end of the roughened region. By $Re_{kk,\,max} \sim 250$, these isolated turbulent wedges had merged circumferentially into a continuous transition front, located well downstream of the origin of the roughness-induced disturbances. Such a response is characteristic of breakdown downstream of a finite-extent "roughness array", or "trip ring", placed on an otherwise smooth surface, as reported by van Driest and Blumer[32] and Boudreau.[33] (Note: in such "trip ring" cases, two regimes are seen: first, ineffective tripping, wherein disturbances input by the isolated roughness elements travel downstream and eventually cause a breakdown to turbulence far removed from the origin of the disturbances; second, effective tripping, wherein the roughness-induced disturbances are sufficient to cause breakdown immediately downstream of the roughness elements.) Continued increases in $Re_{kk,\,max}$ (to 337) resulted in transition fronts that systematically progressed upstream, closer to the beginning of the roughness elements.

Figure 11 summarizes these observations in graphical form. For each experiment, a pair of data points was plotted: $Re_{kk,\,max}$, the maximum roughness Reynolds number that occurred at the start of the roughened zone, and the corresponding $Re_{kk,\,TR}$ that existed at the resulting transition front location. The offset between the two $Re_{kk,}$ values at each $(X/L)_{TR}$ was thus a measure of the "delay" between the initiation of the roughness-induced disturbances and the subsequent breakdown to turbulence.

For $Re_{kk,\,max} \sim 250$, transition occurred at $(X/L)_{TR} \sim 0.5$ at a local roughness Reynolds number of $Re_{kk,\,TR} \sim 150$. Increasing $Re_{kk,\,max}$ (by increasing freestream pressure) caused the transition front to move upstream, occurring at ever-increasing values of $Re_{kk,\,TR}$ (reduced "delays"). Power-law curve fits of each data set, extrapolated to the beginning of the roughness pattern at X/L = 0.2, defined the "effective tripping" limit for the present roughness pattern/model geometry combination (340 ± 6%). In the effective-tripping limit, the transition front is coincident with the onset of the roughness-induced disturbances.

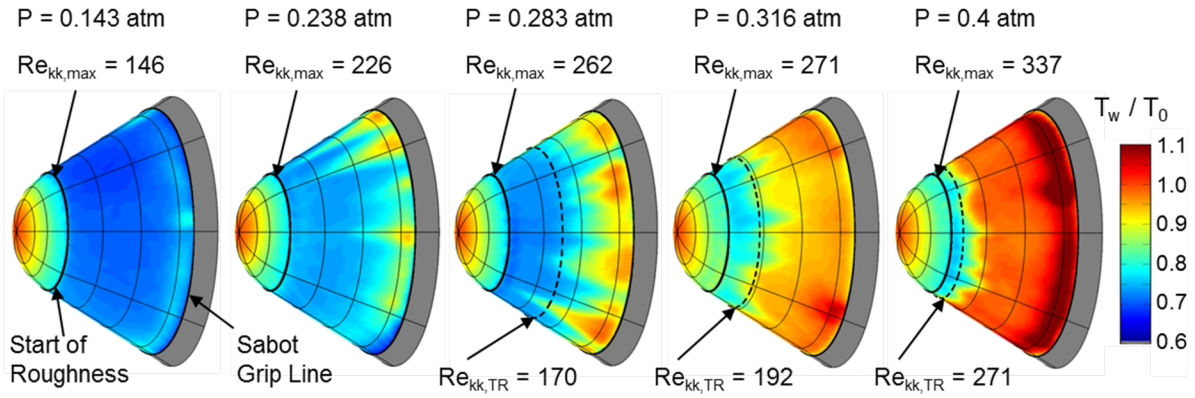

Figure 10. Measured global surface temperature distributions as a function of freestream static pressure; $Re_{kk,max}$ values shown are at the start of roughness, and $Re_{kk,TR}$ values shown are at the measured mean transition front location.

Figure 12 shows measured transition roughness Reynolds numbers for the small-bluntness cones in comparison with those measured for the large-bluntness cones, $\bar{k} = 5.6$ μm for both data sets. The critical roughness Reynolds number concept well describes the small-bluntness data set, but fails to describe the large-bluntness data set.

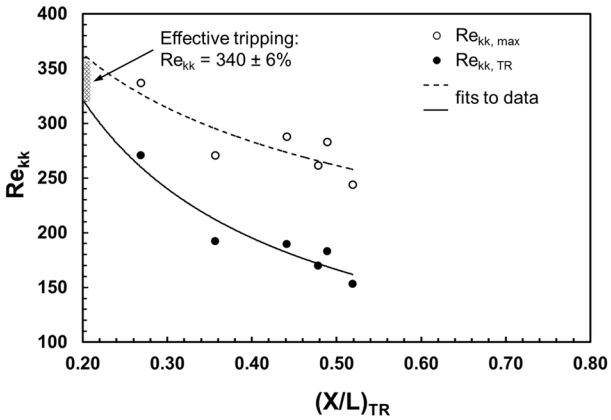

Figure 11. Roughness Reynolds numbers as a function of transition front location on large-bluntness cones with distributed roughness. $Re_{kk} = Re_{kk,max}$ at the start of roughness, and $Re_{kk,TR}$ at the mean transition front location.

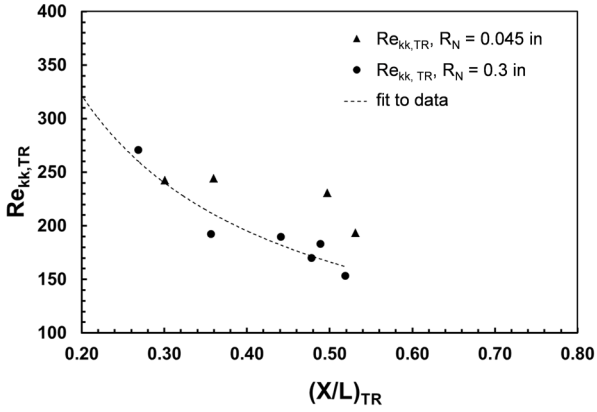

Figure 12. Roughness Reynolds number as a function of transition front location; comparison of small- and large-bluntness cone results. $\bar{k} = 5.6$ μm for both data sets.

V. Conclusions

Thermal images of conical bodies with smooth nosetips and roughened frusta, flown at hypersonic speeds, show that nose bluntness has a major influence on roughness-induced transition onset and progression over the roughened frusta.

For small-bluntness cones, real-gas Navier-Stokes computations of laminar boundary layer development over the model showed that predicted values of the roughness Reynolds number increased with increasing distance from the beginning of the roughness elements. Transition onset was first observed on the roughened frusta near the cone base. Increasing freestream pressure caused the transition front to systematically progress upstream, towards the beginning of the roughened region. At each transition front location, the value of the local roughness Reynolds number was found to be essentially constant, indicating the existence of a critical value for transition (~225 for the $\bar{k} = 5.6$ μm data set).

Conversely, for large-bluntness cones, real-gas Navier-Stokes computations of laminar boundary layer development over the model showed that predicted values of the roughness Reynolds number decreased with

increasing distance from the beginning of the roughness elements. As in the small-bluntness cone experiments, transition was first observed on the roughened frusta near the cone base. However, the local roughness Reynolds number for first occurrence of transition (~150) was considerably lower than the predicted value that existed at the physical beginning of the roughness distribution (~250). Further, this value of ~150 at the transition front was significantly lower than the critical value of ~225 observed for the small-bluntness cones with the same surface roughness. As freestream pressure was increased, the transition front systematically progressed upstream at an ever-increasing value of the local roughness Reynolds number, but this local value at transition was always below the corresponding roughness Reynolds number calculated to exist at the beginning of the roughness distribution. Such a response is similar to that seen in "trip-array" or "trip-ring" applications, wherein a finite extent of roughness elements is placed on an otherwise smooth surface. At low Reynolds numbers, transition first occurs downstream of the trip array, but as Reynolds number is systematically increased, transition moves forward, ultimately reaching the physical location of the trip. This condition is referred to as "effective tripping". Extrapolation of the blunt-cone data to the effective-tripping limit (transition front at X/L = 0.2, for the present experiments) defined an effective-tripping roughness Reynolds number of ~340 ± 6%. For the rough, large-bluntness cones tested herein, the critical roughness Reynolds number concept did not explain observed transition onset values and progression trends.

Acknowledgments

This research was funded by the NASA Fundamental Aeronautics Program, Hypersonics Project, Deepak Bose, Associate Principal Investigator. Dinesh Prabhu is supported by Contract NNA10DE12C from NASA Ames Research Center to ERC, Inc.

References

[1]Pate, S. R. and Schueler, C. J., "Radiated Aerodynamic Noise Effects on Boundary-Layer Transition in Supersonic and Hypersonic Wind Tunnels," *AIAA Journal*, Vol. 7, No. 3, March 1969, pp. 450-457.

[2]Pate, S. R., "Supersonic Boundary-Layer Transition: Effects of Roughness and Freestream Disturbances," *AIAA Journal*, Vol. 9, No. 5, May 1971, pp. 797-803.

[3]Pate, S. R., "Measurements and Correlations of Transition Reynolds Numbers on Sharp Slender Cones at High Speeds," *AIAA Journal*, Vol. 9, No. 6, June 1971, pp. 1082-1090.

[4]Dougherty, N. S., Jr., "Correlation of Transition Reynolds Number with Aerodynamic Noise Levels in a Wind Tunnel at Mach Numbers 2.0-3.0," *AIAA Journal*, Vol. 13, No. 12, December 1975, pp. 1670-1671.

[5]Dougherty, N. S., Jr. and Fisher, D. F., "Boundary-Layer Transition on a 10-Degree Cone: Wind Tunnel/Flight Correlation," AIAA 80-0154, 18th Aerospace Sciences Meeting, Pasadena, CA, January 1980.

[6]Pate, S. R., "Effects of Wind Tunnel Disturbances on Boundary-Layer Transition with Emphasis on Radiated Noise: A Review," AIAA 80-0431, 11th Aerodynamic Testing Conference, Colorado Springs, CO, March 1980.

[7]Pate, S. R., "Dominance of Noise on Boundary Layer Transition in Conventional Wind Tunnels – A Place for the Quiet Ballistic Range in Future Studies," Instability and Transition, Volume I, M. Y. Hussaini and R. G. Voight, Editors, Springer-Verlag, New York, NY, 1990, pp. 77-87.

[8]Reshotko, E., "A Program for Transition Research," *AIAA Journal*, Vol. 13, No. 3, March 1975, pp. 261-265.

[9]Schneider, S. P., "Effects of High-Speed Tunnel Noise on Laminar-Turbulent Transition," *Journal of Spacecraft and Rockets*, Vol. 38, No. 3, May-June 2001, pp. 323-333.

[10]Sheetz, N. W., Jr., "Free-Flight Boundary Layer Transition Investigations at Hypersonic Speeds," AIAA 65-127, 2nd Aerospace Sciences Meeting, New York, NY, January 1965.

[11]Sheetz, N. W., Jr., "Boundary-Layer Transition on Cones at Hypersonic Speeds," AIAA 67-131, 5th Aerospace Sciences Meeting, New York, NY, January 1967.

[12]Sheetz, N. W., Jr., "Ballistics Range Boundary-Layer Transition Measurements on Cones at Hypersonic Speeds," Symposium on Viscous Drag Reduction, LTV Research Center, Dallas, Texas, September 1968, pp. 53-83, Plenum Press, New York, 1969.

[13]Potter, J. L., "Observations on the Influence of Ambient Pressure on Boundary-Layer Transition," *AIAA Journal*, Vol. 6, No. 10, October 1968, pp. 1907-1911.

[14]Potter, J. L., "Boundary-Layer Transition on Supersonic Cones in an Aeroballistic Range," *AIAA Journal*, Vol. 13, No. 3, March 1975, pp. 270-277.

[15]Reda, D. C., "Boundary-Layer Transition Experiments on Sharp Slender Cones in Supersonic Free Flight," *AIAA Journal*, Vol. 17, No. 8, August 1979, pp. 803-810.

[16]Reda, D. C. and Raper, R. M., "Measurements of Transition-Front Asymmetries on Ablating Graphite Nosetips in Hypersonic Flight," *AIAA Journal*, Vol. 17, No. 11, November 1979, pp. 1201-1207.

[17]Reda, D. C., "Comparative Transition Performance of Several Nosetip Materials as Defined by Ballistics-Range Testing," *ISA Transactions*, Vol. 19, No. 1, 1980, pp. 83-98.

[18]Reda, D. C., "Correlation of Nosetip Boundary-Layer Transition Data Measured in Ballistics-Range Experiments," *AIAA Journal*, Vol. 19, No. 3, 1981, pp. 329–339.
[19]Reda, D.C., Wilder, M.C., Bogdanoff, D.W., and Prabhu, D.K., "Transition Experiments on Blunt Bodies with Distributed Roughness in Hypersonic Free Flight", *Journal of Spacecraft and Rockets*, Vol. 45, No. 2, March-April 2008, pp. 210-215.
[20]Reda, D. C., Wilder, M. C., and Prabhu, D. K., "Transition Experiments on Blunt Bodies with Isolated Roughness Elements in Hypersonic Flight," *Journal of Spacecraft and Rockets*, Vol. 47, No. 5, Sep.-Oct. 2010, pp. 828-835.
[21]Reda, D. C., "Review and Synthesis of Roughness-Dominated Transition Correlations for Reentry Applications," *Journal of Spacecraft and Rockets*, Vol. 39, No. 2, March-April 2002, pp. 161-167.
[22]Schiller, L., "Flow in Pipes," *Handbook of Experimental Physics*, Vol. 4, Pt. 4, Academic Press, Leipzig, Germany, 1932, pp. 189-192.
[23]Reshotko, E. and Tumin, A., "Role of Transient Growth in Roughness-Induced Transition", *AIAA Journal*, Vol. 42, No. 4, April 2004, pp. 766-770.
[24]Schneider, S.P. "Effects of Roughness on Hypersonic Boundary-Layer Transition", *Journal of Spacecraft and Rockets*, Vol. 45, No. 2, March-April 2008, pp. 193-209.
[25]Reda, D. C., Wilder, M. C., and Prabhu, D. K., "Transition Experiments on Slightly Blunted Cones with Distributed Roughness in Hypersonic Flight," AIAA 2011-3417, 41st AIAA Fluid Dynamics Conference, Honolulu, HW, June 27-30, 2011 (accepted for publication in *AIAA Journal*).
[26]Wright, M.J., Candler, G.V., and Bose, D., "Data-Parallel Line Relaxation Method for the Navier-Stokes Equations," *AIAA Journal*, Vol. 36, No. 9, 1998, pp. 1603-1609.
[27]Wright, M. J., Bose, D., Palmer, G. E., and Levin, E., "Recommended Collision Integrals for Transport Property Computations Part 1: Air Species," *AIAA Journal*, Vol. 43, No. 12, 2005, pp. 2558-2564.
[28]Wright, M. J., Hwang, H. H., and Schwenke, D., "Recommended Collision Integrals for Transport Property Computations Part II: Mars and Venus Entries," *AIAA Journal*, Vol. 45, No. 1, 2007, pp. 281-288.
[29]Mell, B., "Topography and Roughness Testing of Sandpaper Surface," NANOVEA Technologies Application Note, http://www.nanovea.com/Application%20Notes/SandPaper.pdf, 2010.
[30]Reda, D. C., Wilder, M. C., Bogdanoff, D. W., and Olejniczak, J., "Aerothermodynamic Testing of Ablative Reentry Vehicle Nosetip Materials in Hypersonic Ballistic-Range Environments," AIAA 2004-6829, 1st U.S. Air Force Developmental Test & Evaluation (DT&E) Summit, Woodland Hills, CA, November 16-18, 2004.
[31]Wilder, M. C., Reda, D. C., Bogdanoff, D. W., and Prabhu, D. K., "Free-Flight Measurements of Convective Heat Transfer in Hypersonic Ballistic-Range Environments," AIAA 2007-4404, 39th AIAA Thermophysics Conference, Miami, FL, June 25-28, 2007.
[32]van Driest, E. R. and Blumer, C. B., "Boundary-Layer Transition at Supersonic Speeds: Roughness Effects with Heat Transfer," *AIAA Journal*, Vol.6, No.4, April 1968, pp. 603-607.
[33]Boudreau, A. H., "Artificially Induced Boundary Layer Transition on Blunt-Slender-Cones Using Distributed Roughness and Spherical Type Tripping Devices at Hypersonic Speeds," AIAA 78-1127, 11th Fluid and Plasma Dynamics Conference, Seattle, WA, July 1978.